An Automated Segmentation and Classification Framework for CT-Based Myocardial Perfusion Imaging for Detecting Myocardial Perfusion Defect

Zhen Qian, Parag Joshi, Sarah Rinehart, and Szilard Voros

Piedmont Heart Institute, Piedmont Healthcare, Atlanta, GA, USA

Abstract. Thanks to the recent development of the high-resolution and high-speed multi-sliced CT, CT-based perfusion imaging has become possible. In this paper, we have developed a 320-MDCT-based perfusion imaging framework to detect myocardial ischemia. We designed a rest/stress perfusion imaging protocol, developed an automated LV segmentation algorithm, and adapted a LDA-based classifier to predict myocardial ischemia using the intensity profiles in rest perfusion images. Experiments were done on 6 stress/rest CT perfusion data sets from patients with obstructive coronary artery disease (CAD) and 6 rest CT perfusion data sets from normal subjects. Experimental results have shown that rest perfusion images have the potential of accurately predicting ischemia caused by obstructive CAD.

1 Introduction

Myocardial perfusion imaging is a widely-used cardiovascular diagnostic tool that detects myocardial ischemia and evaluates cardiac function by assessing the blood flow to the heart muscle. Convention myocardial perfusion imaging is based on a nuclear medicine procedure (SPECT), or a first-pass contrast-enhanced MRI. In order to study the reversibility of the myocardial ischemia, myocardial perfusion imaging is usually done at rest and stress, which is induced by physical exercise or drug stimulation.

Cardiac CT is a fast, non-invasive, sub-millimeter resolution imaging modality used to image the heart and the coronary arteries. Thanks to the recent development of the high-resolution and high-speed multi-sliced CT, CT-based perfusion imaging has become possible. Studies [1] [2] have reported that CT-based perfusion imaging on 64- and 256-MDCT single and dual source scanners are predictive of myocardial perfusion defects by visually comparing the myocardial intensity at stress and rest [1] or calculating the transmural perfusion ratio [2]. Compared to nuclear imaging modalities, CT-based perfusion imaging has the potential of achieving higher image resolution and lower radiation dose. Compared to myocardial perfusion MRI, CT technique is more applicable to patients who have metal implants or are too sick to hold their breath for a

D.N. Metaxas and L. Axel (Eds.): FIMH 2011, LNCS 6666, pp. 206–214, 2011.

few heart beats as required by MRI. The additive value of perfusion imaging to imaging the coronary arteries makes cardiac CT a potential "one-stop-shop" procedure for cardiac imaging.

In a recent study [3], a quantitative CT perfusion method on a 320-MDCT was developed. This study demonstrated that CT perfusion at stress and rest is able to quantitatively detect myocardial ischemia by validating against angiography and the measurement of fluid pressure drop caused by the vessel stenosis (fractional flow reserve). Compared to 64- and 256-MDCT, 320-MDCT is unique in cardiovascular imaging: it covers up to $16cm$ length of the scan area in a single gantry rotation. Therefore 320-MDCT is able to scan the whole heart in a single heart beat, and potentially achieve an improved temporal uniformity, or contrast homogeneity, throughout the whole heart. Additionally, 320-MDCT has the potential of lowering the overall contrast media and the overall radiation dose, because it shortens the acquisition time and avoids the helical acquisition.

In this paper, we designed a 320-MDCT-based rest and stress myocardial perfusion imaging protocol and developed an image post-processing framework for the prediction of myocardial ischemia. Fig. 1 shows the flowchart of the framework. The CT perfusion imaging protocol consists of acquiring two sets of contrast-enhanced CT scans of the heart, one at rest and the other under stress, which are acquired 10 minutes apart. We adapted a 3D deformable model-based segmentation algorithm [4] and extended it to a dual-layer structure to segment the endocardial and epicardial surfaces of the left ventricle. The segmented left ventricle is further automatically divided into 17 segments according to the AHA's standard 17-segment model [5]. The intensity profile in each of the 17 segments, as well as in the ventricular blood pool and the whole left ventricle myocardium are derived to train a linear discriminant analysis (LDA)-based classification algorithm to predict ventricular ischemia.

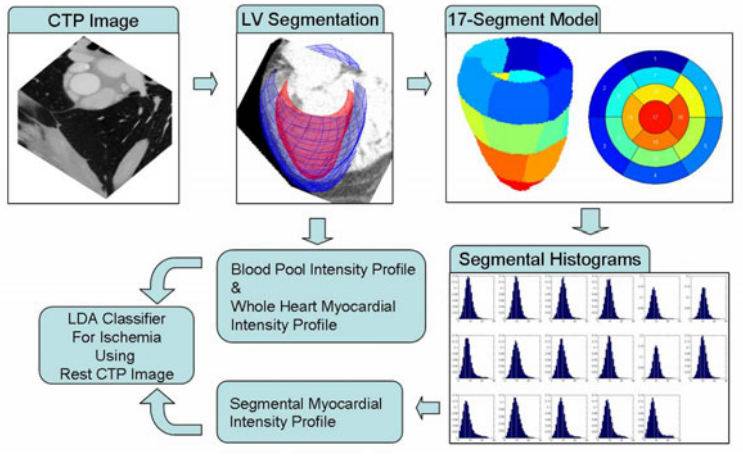

Fig. 1. The flowchart of the CT-based myocardial perfusion imaging framework in predicting myocardial ischemia

In order to validate our proposed approach, in the experiment, we collected 6 CT perfusion data sets from ischemic patients with obstructive coronary artery disease, as defined by invasive angiography and fractional flow reserve. In addition, we also collected 6 normal CT angiography data sets whose imaging protocols are essentially the same as the CT perfusion imaging at rest. In order to avoid unnecessary radiation, we did not acquire stress CT perfusion image on those normal subjects. The myocardial ischemia classifier is trained by using the rest CT perfusion images of those ischemic patients and the normal CT angiography images. Training and testing are done on a strict leave-one-out basis. Experimental results have shown that based on CT rest images, the diagnostic accuracy of ischemia of our method is 91.7% on a strict leave-one-out basis. This suggests CT-based perfusion imaging has the potential to accurately diagnose myocardial ischemia even at rest.

2 Methodology

2.1 CT Perfusion Imaging Protocol

The imaging protocol of the CT-based myocardial perfusion imaging are shown in Fig. 2. The patient first undergoes a rest contrast-enhanced cardiac CT scan with the administration of β-blocker, a medicine that lowers the patient's heart rate. After 10 minutes, the patient undergoes a stress contrast-enhanced cardiac CT scan with the administration of regadenoson, a vasodilator. The detailed imaging parameters for both rest and stress imaging include: 320-MDCT with prospectively triggered, single-beat, volumetric acquisition; detector width was 0.5 mm, voltage was 120 kV, current range was $200 - 550$ mA; reconstruction was done at $65 - 75\%$ R-R. Essentially, the rest CT perfusion protocol is the same as the conventional CT angiography protocol used in clinical practice.

2.2 LV Segmentation in 3D

Much work has been done on myocardial segmentation of the left ventricle in multiple imaging modalities [6].In [7], endocardial surface of the left ventricle was segmented using a Gibbs prior model, a marching-cubes surfacing method, and a local deformable model at the voxel level so that a very detailed surface segmentation can be achieved, including small structures such as the papillary muscles. However, in our application, there is a need to segment the left ventricle,

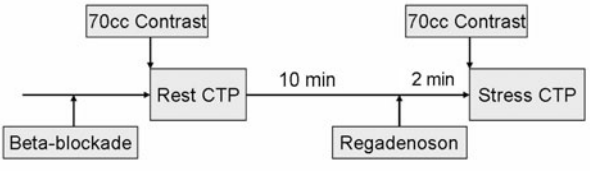

Fig. 2. The imaging protocol of the CT-based myocardial perfusion imaging

including not only the endocardial surface, but also the epicardial surface and the outer boundaries of the left ventricular septum, which is actually part of the endocardial surface of the right ventricle. In addition, there is a need to exclude the papillary muscles and trabeculae structures from the endocardial surface, because the perfusion quantification should be done only in the myocardium. Some of the previous work solved these problems by applying a model to guide the segmentation. In [8], a statistical shape model (ASM) was trained to segment the 4 chambers of the heart. In [9], left ventricle (LV) segmentation was done on a slice-by-slice fashion using morphological operations.

In our study, we did not have a large enough data set to train a model as in [8], and we still needed a strong shape prior to guide the segmentation so that we could exclude the small structures such as the papillary muscle and obtained a smooth boundary surface. Therefore, we adapted a parametric deformable model that consists of two layers of surface meshes, where the distance between the surfaces is constrained by an empirically chosen ventricular thickness. In addition, CT image has a unique characteristic: different tissue has its relatively fixed intensity range in Hounsfield unit (HU). For example, in contrast-enhanced CT image, the myocardium usually has an intensity range of $0 - 250$ HU, while the epicardial fluid and lipid tissue has an intensity below 0 HU. In our approach, the model external force is derived using such characteristic.

Model Initialization. We chose an incomplete ellipsoid shape with rectangular tessellation to model both the endocardial and epicardial surfaces, as illustrated in Fig. 3(a,b). In the surface coordinate system $\mathbf{u} = (u, v)$, $u \in [-\frac{\pi}{2}, \frac{\pi}{4}]$, $v \in [-\pi, \pi)$. In the Cartesian coordinate, the node position $X_o = [x, y, z]'$ can be retrieved by:

$$X_o = \begin{pmatrix} a_x \cos u \cos v \\ a_y \cos u \sin v \\ a_y \sin v \end{pmatrix} \tag{1}$$

where a_x, a_y, and a_z are the scaling parameters in the x, y, and z coordinates.

In contrast-enhanced CT image, the blood pool in the left ventricle is relatively easy to segment because of the increased intensity. We adapt a levelset-based segmentation algorithm [10] to derive the left ventricle blood pool surface first, and use it to guide the model initialization. We denote the nodes of the LV blood surface surface as B_i. As shown in Fig. 3(c), the LV blood pool surface is first manually trimmed to exclude the mitral and aortic valves. Then, the center, long axis orientation and size of B are derived to translate, rotate and scale the surface model in 1. In order to exclude the detailed structure in Fig. 3(c), we impose internal forces of the first and second derivatives of X, and deform the endocardial surface (in red) by iteratively updating $X \leftarrow X + \Delta X$, where,

$$\Delta X = \gamma \cdot F + \alpha(\frac{\partial X}{\partial u} + \frac{\partial X}{\partial v}) + \beta(\frac{\partial^2 X}{\partial u^2} + \frac{\partial^2 X}{\partial v^2}) \tag{2}$$

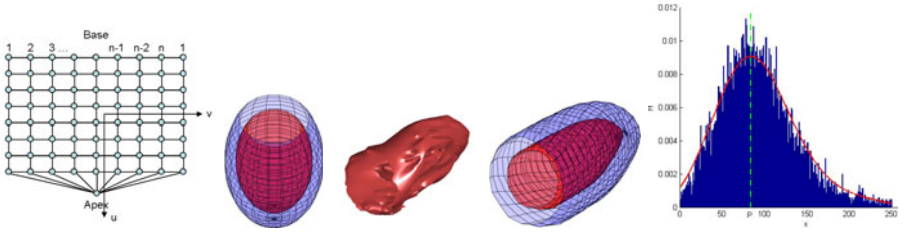

Fig. 3. a) The mesh tessellation. b) The initial parametric model. c) The endo-surface from levelset segmentation. d) the initialized dual-layer surface. e) The intensity histogram is first filtered using a Gaussian filter. Then, the peak location P is found.

where γ, α, β are empirically set weighting parameters that balance the external and internal forces, and F is the external force exerted on the nodes, which is defined by:

$$F = \max_i (N^T \bullet (B_i - X) \cdot N) \tag{3}$$

where N is the outward surface norm of X, and we denote dot product as $\bullet$.

After the endocardial surface is initialized using the blood pool surface, the epicardial surface is initialized by simply expanding the endocardial surface for a certain distance D_o:

$$X_{epi} = X + D_o \cdot N \tag{4}$$

In Fig. 3(d), an example of the initialized endo- and epi-cardial surfaces are illustrated using the LV blood pool surface in Fig. 3(c).

Model Fitting. In the model fitting stage, the deformation update is similar to Equation 2, except for the definition of the external force, which are derived from image intensity profile. The input 3D CT image is first smoothed by a 3D Gaussian filter. Voxel with intensity value off the range of $[0, 250]$ HU are considered off the myocardium, and is replaced with an intensity value of 1000 HU. At each node on the endocardial surface X, we sample a set of the smoothed image intensity value i_m along the outward norm N that is centered at X. The external image force F_{endo} for the endocardial model fitting is defined by:

$$F_{endo} = sign(\operatorname*{argmax}_m \frac{\mathrm{d} \exp \frac{(i_m - \mu)^2}{\sigma^2}}{\mathrm{d}m}) \cdot |\max_m \frac{\mathrm{d} \exp \frac{(i_m - \mu)^2}{\sigma^2}}{\mathrm{d}m})| \tag{5}$$

where μ and σ are empirically selected mean and standard deviation values of the myocardial intensity. Similarly, the external image force F_{epi} for epicardial is defined by:

$$F_{epi} = sign(\operatorname*{argmin}_m \frac{\mathrm{d} \exp \frac{(i_m - \mu)^2}{\sigma^2}}{\mathrm{d}m}) \cdot |\min_m \frac{\mathrm{d} \exp \frac{(i_m - \mu)^2}{\sigma^2}}{\mathrm{d}m})| \tag{6}$$

where the intensity profile is centered at X_{epi}. However, the epicardial surface is more difficult to segment because of the less reliable image information at the

epicardial surface. For instance, it is common that the right ventricle is not filled with contrast, and there is no distinguishable boundary between the septal and the right ventricle blood pool. Therefore, we imposed a stronger internal force that smoothes the inter-surface distance. We define $X_{epi} = X + D$, where X is the endocardial surface, D is the inter-surface distance. We derive X_{epi} by updating $D \leftarrow D + \Delta D$, where

$$\Delta D = \gamma \cdot F_{epi} + \alpha(\frac{\partial D}{\partial u} + \frac{\partial D}{\partial v}) + \beta(\frac{\partial^2 D}{\partial u^2} + \frac{\partial^2 D}{\partial v^2}) \tag{7}$$

2.3 Segmental Intensity Profile

As shown in Fig. 1, the segmented LV is divided into 17 segments using the AHA 17-segment model. In each segment, we first exclude voxels with intensity value off the HU range of $[0, 250]$. Then, the intensity histogram is filtered by a Gaussian filter, and we find the location P of the intensity histogram $H(x)$'s peak, as illustrated in Fig. 3(e). The variation width W of the histogram can be derived by:

$$W = \sqrt{\frac{\sum_x (x - P)^2 \cdot H(x)}{\sum_x H(x)}} \tag{8}$$

2.4 Ischemia Classification Using Linear Discriminant Analysis

In order to investigate the effectiveness of our proposed approach, we adapted a linear discriminant analysis (LDA) [11] algorithm to classify ischemic and normal patients using rest CT perfusion images, because in normal patients, the stress images are not available. A typical two-class LDA classifier can be trained to separate the feature vectors in one class from the other by finding a proper linear projection function. LDA aims to maximizes the between-class scatter and minimizes the within-class scatter. Since in our study, the training sample size is small, we limited the length of the feature vector to avoid over-fitting. We only include the peak location P and variation width W of the blood pool and the whole myocardium, and the variation width W of the segmental myocardial in the feature vector. We did not include the whole intensity histogram profile nor the segmental P values. Therefore, LDA projects the $2+2+17 = 21$ dimensional feature vector to a subspace of $C-1$ dimensions, where C is the number of the classified classes. In this application, $C = 2$. Therefore, the 21 dimensional vector was projected to a 1D scalar. Classification is done by comparing in the 1D subspace, using a k-nearest neighbor scheme. We empirically tested $k = 1$ and 3.

3 Experiments and Results

We collected 6 stress/rest CT perfusion image sets from ischemic patients with obstructive coronary artery disease, and 6 rest CT perfusion image sets from normal subjects. Myocardial perfusion defect is defined by X-ray angiography (XRA) and fractional flow reserve (FFR): XRA $\leq 70\%$ or FFR ≤ 0.75.

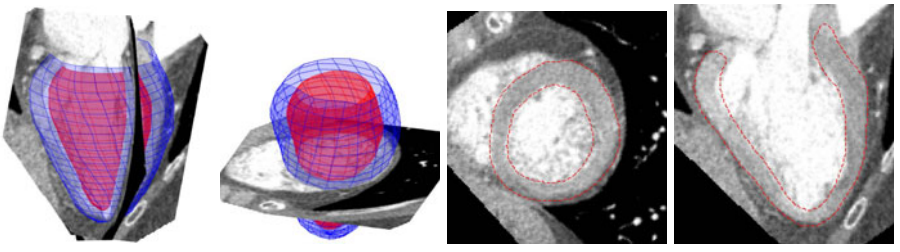

Fig. 4. An example of LV segmentation results in 3D and 2D

3.1 Myocardial Segmentation

We applied our LV myocardial segmentation algorithm on the 6 stress/rest patient data and the 6 rest normal data (18 data sets in total), and obtained very accurate and reliable segmentation results. In Fig. 4, an example of the segmentation results is shown, illustrating that the segmented endocardial surface successfully excludes the papillary muscles from the LV, and the epicardial surface accurately delineates the LV from the epicardial fluid and fat.

Since we do not have manual segmentation results as the ground truth, for quantitative validation, we calculate the percentage of the number of voxels that are off the range of $[0, 250]$ HU in the total voxel number within the segmented LV. Although not exact, this value partially estimates the amount of voxels that are inappropriately included into the LV. From the segmentation results of the 18 data sets, we find the mean and standard deviation of this value are $10.6\% \pm 5.8\%$. Since the LV is a wall structure whose thickness varies in the range of $[0.5, 1.2]$cm in most cases, we can estimate the average combined segmentation error from the endocardial and epicardial surface to be below 1.5mm. In addition, since we excluded all the off-range voxels in the intensity profile analysis and focused on the histogram analysis in the HU range of $[0, 250]$, our experiment shows that such segmentation errors have very limited effects on the subsequent perfusion analysis.

3.2 Visual and Quantitative Assessment of CT Perfusion Image

In the first row of Fig. 5, the stress/rest CT perfusion images from a patient with obstructive left anterior descending artery lesion were shown. The ischemic area, indicated by the red arrow, is easy to visualize in the stress image, but not so apparent in the rest image. In the second row, quantitative analysis shows that the intensity histogram peak location P and variation width W exhibit very similar patterns in the stress and rest perfusion images, but with relatively lower amplitude in the rest images. This suggests that the pattern of intensity profile of the rest CT perfusion image might be potentially predictive of ischemia.

Therefore, we train the LDA classifier using the rest CT perfusion image from 6 ischemic patients and 6 normal subjects. The feature vector of the LDA consists of the P and W of the blood pool in LV and the myocardium in the whole LV, and W of the segmental LV regions. Experiments are done on a strict

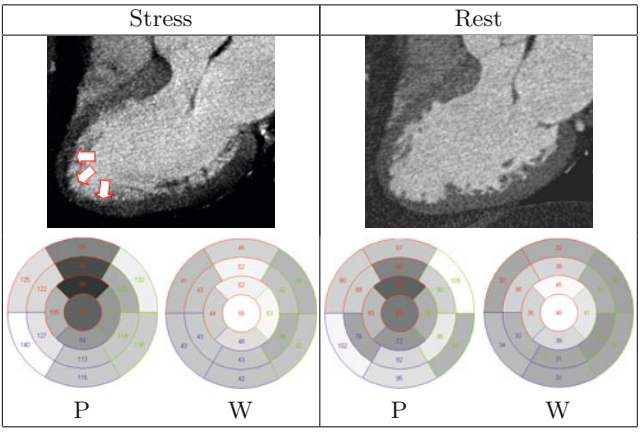

Fig. 5. Visual and quantitative comparison of the stress and rest CT perfusion images

leave-one-out basis, and the LDA classifier accurately classified 11 out 12 data sets, using either $k = 1$ or 3 nearest neighbors.

4 Discussion and Conclusion

In this paper, we have developed a CT-based perfusion imaging framework to detect myocardial ischemia. We designed the rest/stress perfusion imaging protocol for the 320-MDCT, developed an automated LV segmentation algorithm, and adapted a LDA-based classifier to predict myocardial ischemia using the rest perfusion image. Experiments have shown that rest perfusion images have the potential of accurately predicting severe ischemia caused by obstructive CAD. It is probably due to existing myocardial perfusion defects even at rest in those obstructive CAD patients.

There is only one mis-classification in our experiment; however, when substituting that patient's stress image into the LDA testing, the LDA re-classifies it correctly. This suggests that stress imaging amplifies the defects of myocardial perfusion, and in mild to moderately ischemic patients, CT-based stress imaging might be more accurate than rest imaging.

In selecting the feature vector of LDA, we also tested inclusion of the segmental P values, but the accuracy worsens. This may be partially due to the small training sample size. In addition, this suggests the timing of the contrast arriving in the myocardium and then being washed away is difficult to predict and control, which leads to the variation in the overall myocardium intensity levels in CT perfusion images. However, the intensity variation within each local myocardial segment reveals how evenly the blood flow is distributed in the local region, which may be more predictive of obstructive diseases and perfusion defects in the myocardium.

References

1. Blankstein, R., Shturman, L., Rogers, I., et al.: Adenosine-induced stress myocardial perfusion imaging using dual-source cardiac computed tomography. J. Am. Coll. Cardiol. 54, 1072–1084 (2009)
2. George, R., Arbab-Zadeh, A., Miller, J., et al.: Adenosine stress 64- and 256-row detector computed tomography angiography and perfusion imaging: a pilot study evaluating the transmural extent of perfusion abnormalities to predict atherosclerosis causing myocardial ischemia. Circ. Cardiovasc Imaging 2(3), 174–182 (2009)
3. Qian, Z., Vasquez, G., et al.: Validation of quantitative vasodilator stress-rest 320-detector row volumetric ct perfusion imaging against invasive x-ray coronary angiography and fractional flow reserve measurements. In: Annual Scientific Meeting of Society of Cardiovascular Computed Tomography (2010)
4. Metaxas, D.: Physics-Based Deformable Models. Kluwer Academic Publishers, Dordrecht (1996)
5. Cerqueira, M.D., Weissman, N.J., Dilsizian, V., Jacobs, A.K., Kaul, S., Laskey, W.K., et al.: Standardized myocardial segmentation and nomenclature for tomographic imaging of the heart. Circulation 105, 539–542 (2002)
6. Frangi, A., Niessen, W., Viergever, M.: Three-dimensional modeling for functional analysis of cardiac images: A review. IEEE Trans. Med. Imaging 20(1), 2–5 (2001)
7. Chen, T., Metaxas, D., Axel, L.: 3D cardiac anatomy reconstruction using high resolution CT data. In: Barillot, C., Haynor, D.R., Hellier, P. (eds.) MICCAI 2004. LNCS, vol. 3216, pp. 411–418. Springer, Heidelberg (2004)
8. Zheng, Y., Georgescu, B., Barbu, A., Scheuering, M., Comaniciu, D.: Four-chamber heart modeling and automatic segmentation for 3D cardiac CT volumes. In: SPIE, Medical Imaging, vol. 6914 (2008)
9. Silva, S., Sousa Santos, B., Madeira, J., Silva, A.: Left ventricle segmentation from heart MDCT. In: Araujo, H., Mendonça, A.M., Pinho, A.J., Torres, M.I. (eds.) IbPRIA 2009. LNCS, vol. 5524, pp. 306–313. Springer, Heidelberg (2009)
10. Li, C., Huang, R., Ding, Z., Gatenby, C., Metaxas, D., Gore, J.: A variational level set approach to segmentation and bias correction of images with intensity inhomogeneity. In: Metaxas, D., Axel, L., Fichtinger, G., Székely, G. (eds.) MICCAI 2008, Part II. LNCS, vol. 5242, pp. 1083–1091. Springer, Heidelberg (2008)
11. Martinez, A.M., Kak, A.C.: PCA versus LDA. IEEE Trans. on Pattern Analysis and Machine Intelligence 23(2), 228–233 (2001)